Inhibiting Cxcr2 disrupts tumor-stromal interactions and improves survival in a mouse model of pancreatic ductal adenocarcinoma

Hideaki Ijichi,[1] Anna Chytil,[2,3] Agnieszka E. Gorska,[2,3] Mary E. Aakre,[2,3] Brian Bierie,[4] Motohisa Tada,[1,5] Dai Mohri,[1] Koji Miyabayashi,[1] Yoshinari Asaoka,[1] Shin Maeda,[6] Tsuneo Ikenoue,[7] Keisuke Tateishi,[1] Christopher V.E. Wright,[8,9] Kazuhiko Koike,[1] Masao Omata,[1,10] and Harold L. Moses[2,3]

[1]Department of Gastroenterology, Graduate School of Medicine, University of Tokyo, Tokyo, Japan. [2]Department of Cancer Biology and [3]Vanderbilt-Ingram Comprehensive Cancer Center, Vanderbilt University, Nashville, Tennessee, USA. [4]Whitehead Institute for Biomedical Research, Cambridge, Massachusetts, USA. [5]Department of Medicine and Clinical Oncology, Graduate School of Medicine, Chiba University, Chiba, Japan. [6]Department of Gastroenterology, Graduate School of Medicine, Yokohama City University, Kanagawa, Japan. [7]Division of Clinical Genome Research, Institute of Medical Sciences, University of Tokyo, Tokyo, Japan. [8]Cell and Developmental Biology and [9]Vanderbilt University Program in Developmental Biology, Vanderbilt University, Nashville, Tennessee, USA. [10]Yamanashi Prefectural Central Hospital, Yamanashi, Japan.

Pancreatic ductal adenocarcinoma (PDAC), one of the most lethal neoplasms, is characterized by an expanded stroma with marked fibrosis (desmoplasia). We previously generated pancreas epithelium–specific TGF-β receptor type II (Tgfbr2) knockout mice in the context of Kras activation (mice referred to herein as Kras+Tgfbr2^{KO} mice) and found that they developed aggressive PDAC that recapitulated the histological manifestations of the human disease. The mouse PDAC tissue showed strong expression of connective tissue growth factor (Ctgf), a profibrotic and tumor-promoting factor, especially in the tumor-stromal border area, suggesting an active tumor-stromal interaction. Here we show that the PDAC cells in Kras+Tgfbr2^{KO} mice secreted much higher levels of several Cxc chemokines compared with mouse pancreatic intraepithelial neoplasia cells, which are preinvasive. The Cxc chemokines induced Ctgf expression in the pancreatic stromal fibroblasts, not in the PDAC cells themselves. Subcutaneous grafting studies revealed that the fibroblasts enhanced growth of PDAC cell allografts, which was attenuated by Cxcr2 inhibition. Moreover, treating the Kras+Tgfbr2^{KO} mice with the CXCR2 inhibitor reduced tumor progression. The decreased tumor progression correlated with reduced Ctgf expression and angiogenesis and increased overall survival. Taken together, our data indicate that tumor-stromal interactions via a Cxcr2-dependent chemokine and Ctgf axis can regulate PDAC progression. Further, our results suggest that inhibiting tumor-stromal interactions might be a promising therapeutic strategy for PDAC.

Introduction

Pancreatic cancer is the fourth and fifth leading cause of cancer death in the United States and Japan, respectively (1, 2). It is one of the most lethal cancers, with 5-year survival rate of less than 5% that is partially attributed to the difficulty of early diagnosis. Moreover, even with a successful resection, 5-year survival is still less than 20%. The poor outcome after resection may be due to the frequent aggressive character of pancreatic tumor cells, which are often able to efficiently invade, disseminate, and metastasize (3, 4).

The most common type of human pancreatic cancer is pancreatic ductal adenocarcinoma (PDAC). Previous studies have suggested a multistep progression model of PDAC that includes a preinvasive state termed pancreatic intraepithelial neoplasia (PanIN). PDAC is thought to result from progression of PanIN lesions through accumulation of specific genetic alterations (5). Activation of a point mutation of the *KRAS* proto-oncogene and inactivation of tumor suppressor genes, including *P16^{INK4A}*, *P53*, and *SMAD4* (also known as deleted in pancreatic adenocarcinoma 4 [*DPC4*]), have been shown to increase in frequency with progression of the PanIN stages. Notably, at the invasive stage, the mutations and deletions of *KRAS*, *P16^{INK4A}*, *P53*, and *SMAD4* are found in approximately 90%, 90%, 75%, and 55% of PDAC, respectively (6). Therefore, alteration of these signaling pathways may have a causal or permissive role that allows progression from PanIN to PDAC in vivo.

Genetically engineered murine PDAC progression models have recently been described by using pancreas-specific conditional activation or knockout of clinically relevant PDAC-related genes and signaling pathways (7–11). Pancreas epithelium–specific expression of active *Kras* was shown to result in murine PanIN (mPanIN) (7). Importantly, inactivation of tumor suppressor genes *p16^{INK4a}* (8), *p53* (9, 10), or *Tgfbr2* (TGF-β receptor type II) (11) dramatically accelerated PDAC progression in the context of *Kras* activation. These models all followed a multistep model of disease progression through mPanIN and developed aggressive invasive PDAC. However, in the *p16^{INK4a}* knockout model and *p53* inactivation model, the PDAC was frequently accompanied by sarcomatoid or undifferentiated components, which are infrequent in human pancreatic cancer (8–10). In contrast, the *Tgfbr2* knockout model was largely comprised of differentiated PDAC without the undifferentiated histology (11).

Mutation of the *TGFBR2* gene is less common when compared with *SMAD4* (12), both of which are signaling components in the TGF-β signaling pathway. However, nearly half of PDAC cases may have decreased *TGFBR2* expression, according to previous reports

Conflict of interest: The authors have declared that no conflict of interest exists.
Citation for this article: *J Clin Invest.* 2011;121(10):4106–4117. doi:10.1172/JCI42754.

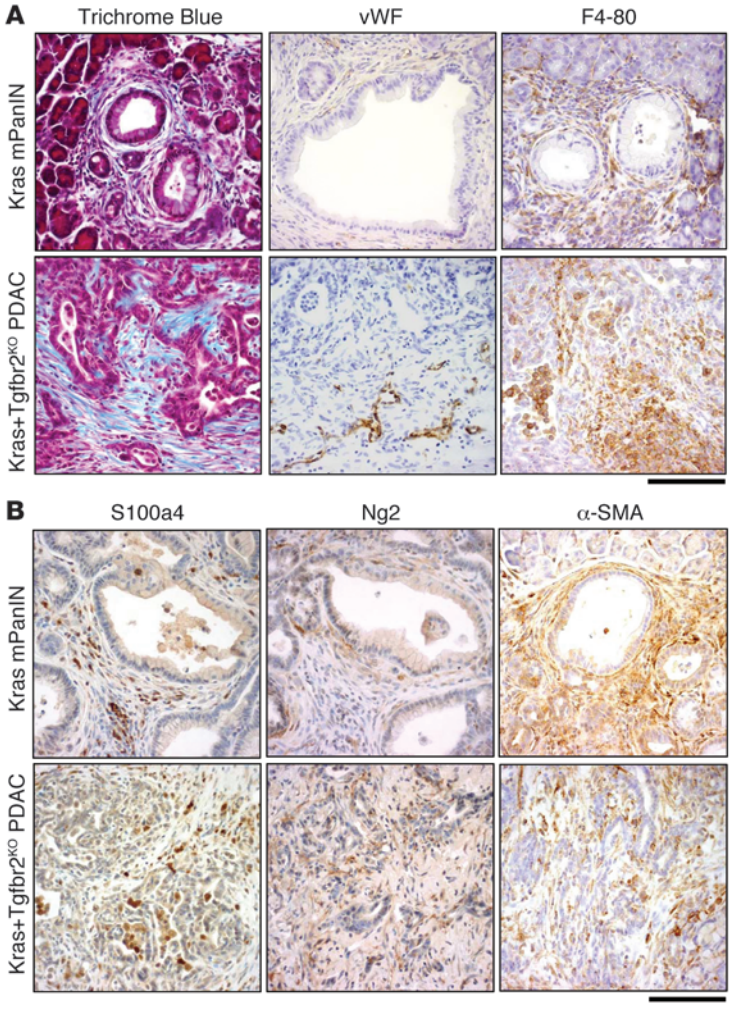

Figure 1
Stromal components in *Ptf1a*$^{cre/+}$*;LSL-Kras*$^{G12D/+}$*;Tgfbr2*$^{flox/flox}$ PDAC and *Ptf1a*$^{cre/+}$*;LSL-Kras*$^{G12D/+}$ mPanIN tissue. (**A**) *Ptf1a*$^{cre/+}$*;LSL-Kras*$^{G12D/+}$*;Tgfbr2*$^{flox/flox}$ PDAC stroma demonstrated prominent collagen deposition with Trichrome Blue staining and abundant macrophage and histiocyte infiltration with F4-80 immunostaining. PDAC also showed positive vascular endothelial cell staining with von Willebrand factor immunostaining, specifically in the invasion front area. *Ptf1a*$^{cre/+}$*;LSL-Kras*$^{G12D/+}$ mPanIN stroma also showed stromal expansion to a lesser extent. (**B**) Fibroblast antigens (S100a4, Ng2, α-SMA) were abundantly observed in the stroma of both mPanIN and PDAC. Scale bars: 125 μm.

(13, 14). Therefore, TGF-β–SMAD signaling is impaired in most PDACs. Recently, studies of pancreatic epithelium–specific *Smad4* knockout models in the context of active *Kras* expression were also published (15–17). Interestingly, these models showed mucinous cystic neoplasia and intraductal papillary mucinous neoplasia, rather than PDACs that occur through stepwise mPanIN progression, suggesting that the murine model of *Kras* activation with *Tgfbr2* knockout (Kras+Tgfbr2^{KO}) might provide the closest approximation of histological features that frequently occur in human PDAC. In addition it has been shown that xenograft tumor models, which have been frequently used in studies of tumor progression, are quite different from the human disease with regard to tumor vasculature and drug delivery (18). Thus, use of the Kras+Tgfbr2^{KO} autochthonous tumor model is likely to provide useful results for clinical application.

The Kras+Tgfbr2^{KO} PDAC demonstrated abundant stromal components in the tumor tissue and recapitulated desmoplasia, a hallmark in human PDAC histology, which is defined as proliferation of fibrotic and connective tissue around the invasive tumor (11). Recent studies suggested that the desmoplastic reaction can favor tumor progression and chemoresistance (19–21). The fact that PDAC and scirrhous type gastric cancer, which is also well known for its invasiveness and poor prognosis, both exhibit the desmoplasia as a distinguishing feature supports the pro-invasive role for this reaction during cancer progression. Unfortunately, at present little is known about how pancreatic tumor cells interact with the adjacent stromal cells during tumor progression and metastasis. However, the tumor-stromal interactions during tumor progression are likely significant, and therefore paracrine mediators of this interaction are rational candidates for targeted adjuvant therapy.

In the present study, we show that PDAC cells can secrete several Cxc chemokines into the tumor microenvironment at a significantly higher level than mPanIN cells. The chemokines stimulated stromal fibroblasts to induce connective tissue growth factor (Ctgf), a pro-fibrotic and tumor-promoting factor. The tumor-stromal interaction accelerated tumor growth in vivo. The tumors were shown to progress in a Cxcr2-dependent manner, and inhibiting the chemokine-Cxcr2 axis had a significant antitumor effect. Further, Cxcl-Cxcr2 inhibition extended the survival of Kras+Tgfbr2^{KO} PDAC mice by inhibiting tumor angiogenesis. These results suggest that inhibiting tumor-stromal interactions, and more specifically the Cxcl-Cxcr2 axis, could be a promising therapeutic strategy for PDAC, the most lethal human cancer.

Results

Mouse PDAC tissue contains abundant stromal components. The *Ptf1a*$^{cre/+}$*;LSL-Kras*$^{G12D/+}$*;Tgfbr2*$^{flox/flox}$ PDAC demonstrated remarkable stromal tissue expansion in the tumor, which resembled human PDAC (Figure 1). In addition to the previously reported abundant vimentin and α–smooth muscle actin staining, both of which mark most mesenchymal cells, Trichrome staining revealed abundant collagen deposition in the expanded stroma. Moreover, S100a4 (also known as fibroblast-specific protein [Fsp]) and Ng2 staining, both of which mark fibroblasts, also demonstrated fibroblast-rich mesenchyme in PDAC tumors. Abundant stroma, especially fibrosis associated with invasive carcinoma (desmoplasia), is one of the features of human PDAC, and the *Ptf1a*$^{cre/+}$*;LSL-Kras*$^{G12D/+}$*;Tgfbr2*$^{flox/flox}$ PDAC recapitulated it very well.

In addition to the desmoplastic reaction, von Willebrand factor staining (which detects endothelial cells) showed tumor angiogenesis that was preferentially localized in the periphery of PDAC tumors, while little signal was detected within the central mass of PDAC tumor tissues. This feature was also consistent with human PDAC tissues, which are almost always hypovascular. Notably, F4-80 staining revealed abundant macrophage and histiocyte infiltration in the PDAC tissue, which was also observed in early mPanIN lesions from the *Ptf1a*$^{cre/+}$*;LSL-Kras*$^{G12D/+}$ model, suggesting the infiltration is an early event during progression.

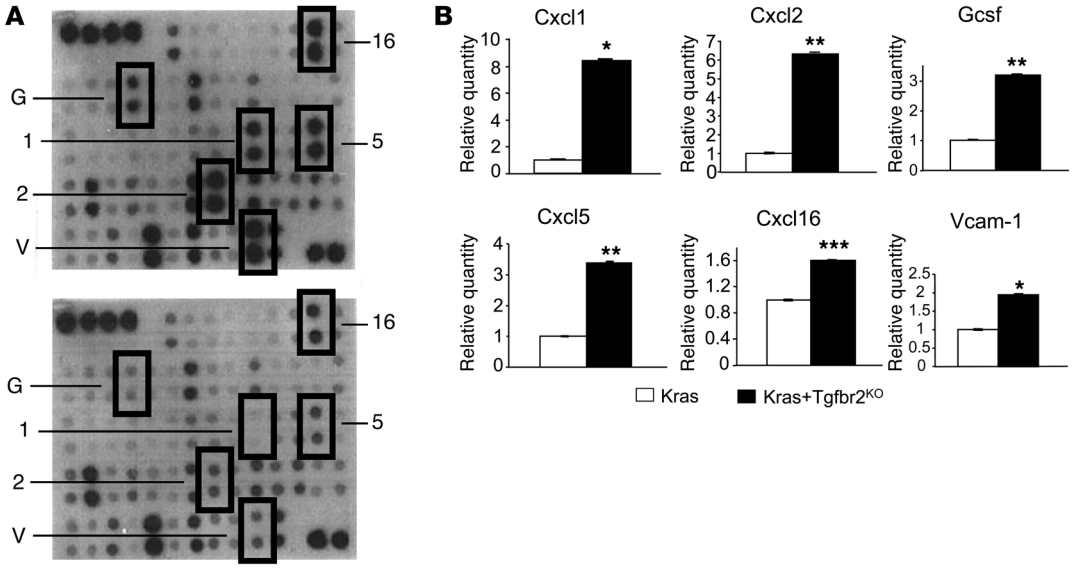

Figure 2

Ptf1a$^{cre/+}$*;LSL-Kras*$^{G12D/+}$*;Tgfbr2*$^{flox/flox}$ PDAC cells produce and secrete Cxc chemokines and other soluble factors into the tumor microenvironment. (**A**) A representative mouse cytokine array using CM from a *Ptf1a*$^{cre/+}$*;LSL-Kras*$^{G12D/+}$*;Tgfbr2*$^{flox/flox}$ PDAC cell line (top) and a *Ptf1a*$^{cre/+}$*;LSL-Kras*$^{G12D/+}$cell line (bottom). 1, Cxcl1; 2, Cxcl2; 5, Cxcl5; 16, Cxcl16; G, Gcsf; V, Vcam-1. (**B**) Quantification of the mouse cytokine array data. The data from Kras mPanIN cells were set as 1, and relative quantity is shown. Kras+Tgfbr2^{KO} PDAC cells secreted higher levels of Cxc chemokines and other soluble proteins compared with Kras mPanIN cells. Kras indicates *Ptf1a*$^{cre/+}$*;LSL-Kras*$^{G12D/+}$ mPanIN cell lines; Kras+Tgfbr2^{KO} indicates *Ptf1a*$^{cre/+}$*;LSL-Kras*$^{G12D/+}$*;Tgfbr2*$^{flox/flox}$ PDAC cell lines. **P* < 0.05; ***P* < 0.01; ****P* < 0.001.

PDAC cells produce Cxc chemokines and other secreted factors into the tumor microenvironment. The abundant stroma in PDAC tumors suggested that tumor-stromal interactions may be an important factor worth consideration in the PDAC tumor microenvironment. We hypothesized that PDAC cells may produce and release certain factors into the microenvironment and the stromal cells could in turn respond to these factors. Therefore, through a productive tumor-stromal interaction, tumor cells can establish favorable circumstances for themselves, resulting in selection and dissemination of tumor cells that are resistant to conventional therapies.

To screen for secreted factors produced by the PDAC cells, we isolated them from the *Ptf1a*$^{cre/+}$*;LSL-Kras*$^{G12D/+}$*;Tgfbr2*$^{flox/flox}$ PDAC tissue as well as mPanIN cells from the *Ptf1a*$^{cre/+}$*;LSL-Kras*$^{G12D/+}$ pancreas tissue as described previously (11). We confirmed the *Kras* allele recombination both in the PDAC and mPanIN cells and *Tgfbr2* allele recombination only in the PDAC cells (Supplemental Figure 1; supplemental material available online with this article; doi:10.1172/JCI42754DS1). Both cells also showed ERK phosphorylation, indicating Kras-ERK signal activation (Supplemental Figure 1). We then performed cytokine antibody array analyses using conditioned media (CM) from the isolated cells. As shown in Figure 2, several chemokines, cytokines, and cell surface proteins were released from the PDAC cells at a significantly higher level when compared with the mPanIN cells. Among the upregulated secretory proteins, Cxc chemokines Cxcl1, Cxcl2, Cxcl5, and Cxcl16 were noteworthy. Quantitative RT-PCR (QRT-PCR) revealed that Cxcl1, Cxcl5, and Cxcl16 were upregulated in the PDAC cells, which confirmed that in addition to increased protein secretion, these chemokines were upregulated at transcriptional level as well (Figure 3A).

To assess whether the transcription of those chemokines could be downregulated by TGF-β signaling, the mPanIN cells, which have intact Tgfbr2 expression, were stimulated with TGF-β1 (Figure 3B). Although basal transcription level of the Cxc chemokines was extremely low in mPanIN cells when compared with the PDAC cells, the Cxcl1 and Cxcl5 expression was significantly decreased by TGF-β1 treatment, suggesting that these chemokines were directly regulated by TGF-β signaling. However, Cxcl16 expression did not decrease by TGF-β1 treatment (data not shown), which suggested that Cxcl16 was not a direct target gene of TGF-β signaling (rather, it may be regulated by TGF-β through a more complex indirect mechanism). We also treated the Kras+Tgfbr2^{KO} PDAC cells with TGF-β1, but those cells did not show downregulation of Cxcl1 and -5 (Figure 3B), which was consistent with the idea that TGF-β signaling was already disrupted in those cells.

Next we examined the underlying signal mechanism of Cxc chemokine upregulation by TGF-β signal blockade. We performed QRT-PCR of Cxcl1 and -5 using the Kras+Tgfbr2^{KO} PDAC cells incubated with various representative signal inhibitors, including U1026 for ERK, LY294002 for PI3K, SP600125 for JNK, SB203580 for p38MAPK, and SC-514 for NF-κB signal inhibition, respectively. Among these, the NF-κB inhibitor SC-514 (an IκB kinase-2 inhibitor) showed a significant suppression of the Cxcl1 and -5 expression (Figure 3C), but other inhibitors did not (Supplemental Figure 2). This indicated that the Cxcl upregulation was NF-κB signal dependent and suggested that TGF-β signal had an inhibitory effect on NF-κB signal in the normal and precancer cells.

The Cxcl-Cxcr2 axis is associated with tumor-stromal interactions in the PDAC tumor microenvironment. The CXC chemokines CXCL1, CXCL2, and CXCL5 all bind to CXCR2, and CXCL16 binds to CXCR6. Therefore, we hypothesized that the CXCL1, 2, 5-CXCR2 and CXCL16-CXCR6 axes might be important regulators of PDAC progression. Immunohistochemistry of Cxcl1 revealed high expression of the ligand in the Kras+Tgfbr2^{KO} PDAC tissue (Figure 4A).

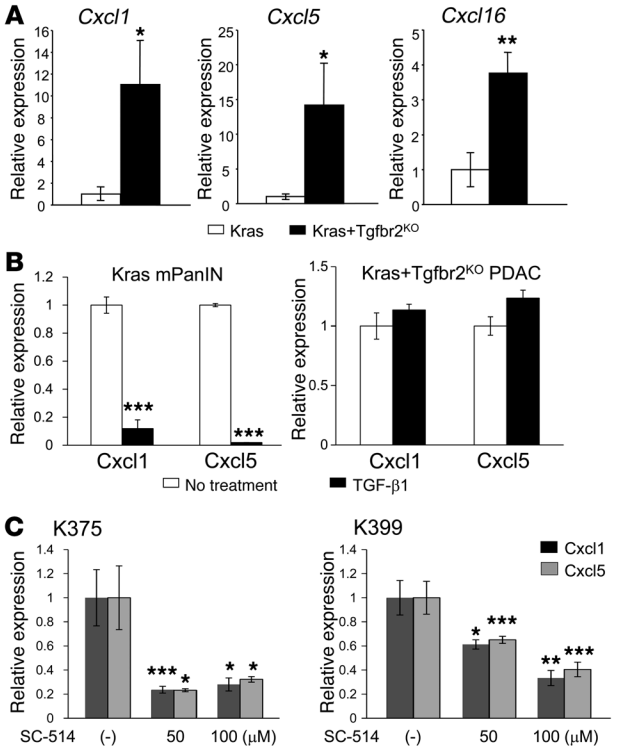

Figure 3

Transcriptional regulation of Cxc chemokines in the PDAC and mPanIN cells. (**A**) Cxc chemokines were upregulated at the mRNA level in the Kras+Tgfbr2^{KO} PDAC cells compared with Kras mPanIN cells in QRT-PCR analysis. The data of Kras mPanIN cells was assigned as 1, and relative quantity is shown. (**B**) *Cxcl1* and *-5* mRNA expression was downregulated by TGF-β signaling in the Kras mPanIN cell lines, but not in the Kras+Tgfbr2^{KO} PDAC cells. Cells were incubated with or without 5 ng/ml TGF-β1 for 6 hours, and QRT-PCR was performed. The data without TGF-β1 was assigned as 1, and relative quantity is shown. (**C**) The upregulation of Cxcl1 and -5 in Kras+Tgfbr2^{KO} PDAC cells was NF-κB signal dependent. Kras+Tgfbr2^{KO} PDAC cells (K375 and K399) were incubated with NF-κB inhibitor SC-514 (0–100 μM) for 12 hours, and QRT-PCR was performed. Data without an inhibitor were set as 1, and relative quantity is shown. *$P < 0.05$; **$P < 0.01$; ***$P < 0.001$.

Although the receptor Cxcr2 was detected in the normal and mPanIN pancreas epithelia, the expression was relatively prominent at the invasive front of the PDAC tissue, in both the stroma and epithelium (Figure 4A).

We examined whether the Cxc chemokines promote the PDAC cell proliferation in vitro in an autocrine manner by using various concentrations of the CXCR2 inhibitor SB225002. However, Cxcr2 inhibition did not influence the PDAC cell proliferation (Figure 4B). As a result, we hypothesized that these Cxc chemokines may have an impact on the stromal cell response rather than acting as autocrine regulators of PDAC cells.

To address the potential tumor-stromal interaction between the PDAC cells and adjacent fibroblasts, we isolated fibroblasts from *Ptf1a$^{cre/+}$;LSL-Kras$^{G12D/+}$* pancreas. The fibroblasts were morphologically identified and characterized by PCR, Western blot, and immunostaining (Figure 4, C and D, and data not shown). Western blot demonstrated abundant S100a4 (Fsp) protein expression in the fibroblasts, while the PDAC cells were negative for the stromal marker protein (Figure 4C). Immunofluorescence also elucidated that the fibroblasts were negative for ZO-1 cell–junctional staining and strongly positive for stress fiber formation. These results confirmed that the cells examined were derived from the stromal fibroblast population. When cytokeratin-19 (CK19) was detected by immunocytochemistry as a ductal epithelial marker, the isolated fibroblast cells were CK19 negative, whereas both the PDAC and mPanIN cells described above were CK19 positive, which was consistent with their derivation (data not shown).

Cxcr2 expression was examined in the PDAC cells, mPanIN cells, and pancreatic fibroblasts using QRT-PCR, which revealed that the mRNA expression level was significantly higher than the tumor epithelial cells in isolated fibroblasts (Figure 4E). Cxcr2 immunohistochemistry showed relatively prominent staining at the invasive front of the PDAC in both the stroma and the epithelium (Figure 4A), although Cxcr2 inhibition did not affect PDAC cell proliferation in vitro (Figure 4B). Taken together, these data suggest that Cxcr2 chemokine ligands secreted from the PDAC cells can have an impact on stromal fibroblasts and this tumor-stromal interaction could have a significant impact on PDAC progression.

MMP-2 was previously described as important in the PDAC tumor microenvironment, especially in terms of promoting metastasis and invasion (21, 22). However, in the present study neither antibody array nor QRT-PCR detected a significant increase of MMP production by the PDAC cells when compared with mPanIN cells (data not shown), suggesting that the differential impact of MMPs on tumor progression was not a significant factor in this PDAC model.

Cxc chemokines from PDAC cells induce Ctgf expression in the pancreatic fibroblasts. Previously, we reported that Ctgf was strongly expressed at the tumor-stromal border of *Ptf1a$^{cre/+}$;LSL-Kras$^{G12D/+}$;Tgfbr2$^{flox/flox}$* PDAC tissues (11). CTGF has been reported recently to have tumor-promoting activities (23–26). In this study, using a more specific Ctgf antibody, we found again strong Ctgf staining at the tumor-stromal border (Figure 5A). This suggested that an active Ctgf-dependent tumor-stromal interaction was present in the PDAC tissue that could be a therapeutic target, since the interaction increased in intensity during tumor progression.

This observation prompted us to examine whether the Cxc chemokines from PDAC cells could induce Ctgf expression in the stromal fibroblasts. QRT-PCR showed that the fibroblasts had much higher basal expression of *Ctgf* mRNA compared with the PDAC cells and the expression was significantly upregulated when the cells were stimulated with Cxcl1, Cxcl2, and Cxcl5 (Figure 5B). Next, we incubated the fibroblasts with the CM from PDAC cells, mPanIN cells, or control media without cells. As shown in Figure 5C, the PDAC CM induced significantly higher expression level of

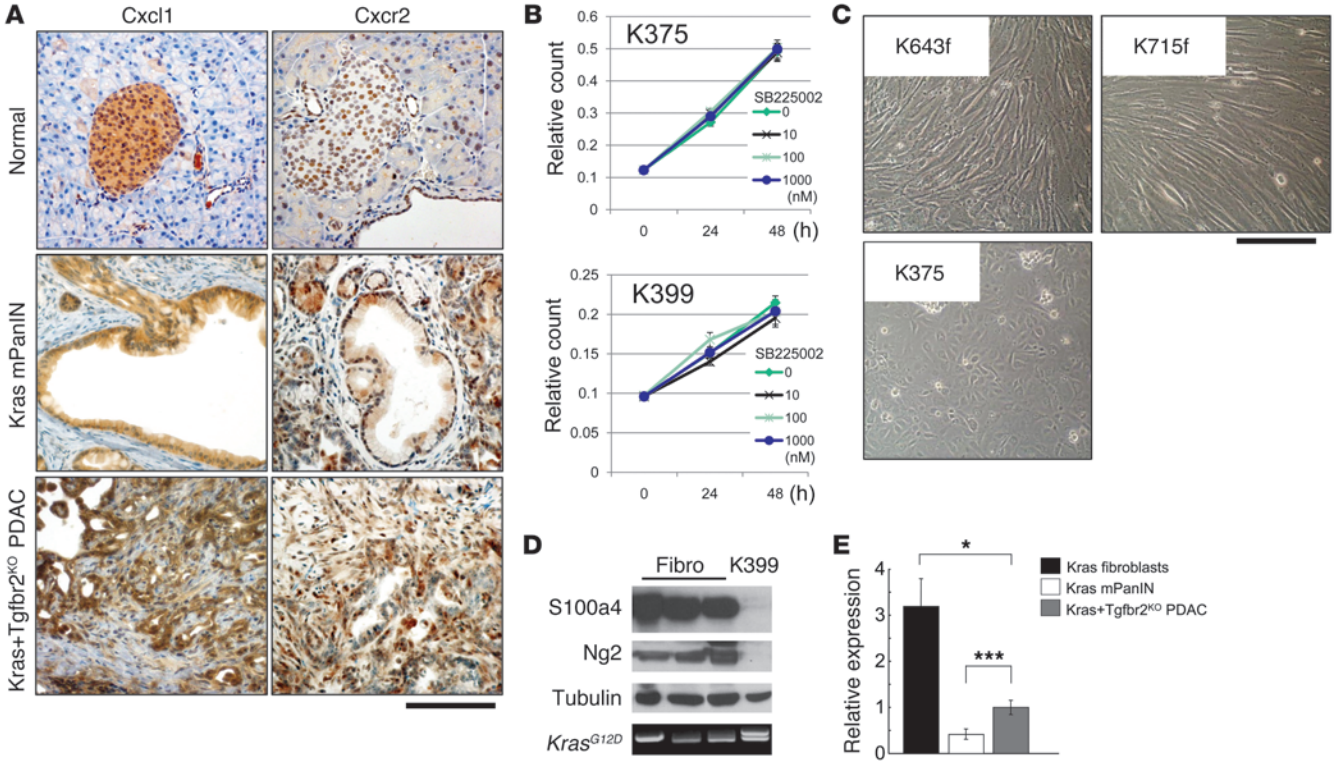

Figure 4

The Cxcl1-Cxcr2 axis might be important in the tumor-stromal interaction in the PDAC tumor microenvironment. (**A**) Immunohistochemistry of Cxcl1 and Cxcr2 in Kras+Tgfbr2^{KO} PDAC, Kras mPanIN, and normal pancreas tissue. PDAC tissue showed more abundant expression of Cxcl1 and Cxcr2. Cxcl1 was expressed mainly in the epithelial cells. Cxcr2 was also positive in the epithelial cells, and the staining was relatively prominent at the invasive front of PDAC, both in the epithelium and stroma. Scale bar: 125 μm. (**B**) Cxcr2 inhibition did not change proliferation of the Kras+Tgfbr2^{KO} PDAC cells. Cell proliferation assay of the Kras+Tgfbr2^{KO} PDAC cells (K375, K399) with 0–1 μM SB225002, a CXCR2 inhibitor, demonstrated no inhibition with any concentration of SB225002. (**C**) Representative photomicrographs of *Ptf1a$^{cre/+}$;LSL-Kras$^{G12D/+}$* fibroblasts (K643f, K715f) and Kras+Tgfbr2^{KO} PDAC cells (K375). Scale bar: 125 μm. (**D**) Western blotting showed that *Ptf1a$^{cre/+}$;LSL-Kras$^{G12D/+}$* fibroblasts (fibro) expressed fibroblast antigens (S100a4, Ng2), while the Kras+Tgfbr2^{KO} PDAC cells (K399) did not. Tubulin was used as a loading control. Genomic DNA PCR showed *Kras* allele recombination (top band) in Kras+Tgfbr2^{KO} PDAC cells but not in *Ptf1a$^{cre/+}$;LSL-Kras$^{G12D/+}$* fibroblasts. (**E**) QRT-PCR showed much higher *Cxcr2* mRNA expression in fibroblasts compared with epithelial cells in the pancreas. Data from Cxcr2 expression in Kras+Tgfbr2^{KO} PDAC cells were set as 1, and relative quantity is shown. *$P < 0.05$; ***$P < 0.001$.

Ctgf mRNA compared with mPanIN CM. CXCR2 inhibitors repertaxin (27) and SB225002 inhibited the PDAC CM–induced Ctgf upregulation in a dose-dependent manner (Figure 5C). Since TGF-β signaling is well known to induce Ctgf expression, we examined whether the Cxcl-induced Ctgf expression in the pancreatic fibroblasts was also TGF-β signal dependent. Tgfbr1 inhibitor SB431542 dramatically suppressed the Ctgf induction, which indicated that Ctgf induction by Cxcls was also TGF-β signal dependent. Taken together, the data suggest that Cxc chemokines produced by PDAC cells can stimulate pancreatic fibroblasts to express Ctgf in a Cxcr2 signal–dependent and TGF-β signal–dependent manner. We also examined proliferation of the pancreatic fibroblasts with and without the PDAC CM in vitro, but the proliferation was not accelerated with the PDAC CM (data not shown).

The tumor-stromal interaction between PDAC cells and pancreatic fibroblasts promotes PDAC subcutaneous tumor growth in a Cxcr2 signal–dependent manner in vivo. Results obtained in vitro do not always reflect the situation in vivo. Therefore, it was imperative that we determine whether the PDAC-derived chemokine tumor-stromal signaling axis was functionally relevant in vivo. To address this issue, we performed subcutaneous injections into nude mice with 3×10^6 PDAC cells (K399) alone (group A) or with a mixture of 1.5×10^6 PDAC cells (K399) and 1.5×10^6 pancreatic fibroblasts (K643f) (group B), then compared the in vivo tumor growth. Subcutaneous injection with the pancreatic fibroblasts (K643f) alone did not produce tumors. Since K643f was isolated from the activated-Kras mouse pancreas, which contained only mPanIN tissue, it was not considered a true cancer-associated fibroblast line. To exclude the possibility that the fibroblast population obtained from PDAC tissue still contained a small amount of PDAC cells, which could propagate tumor formation in vivo, we used the relatively normal fibroblasts in this study. In this simplified condition, although the number of PDAC cells in group B was half of the number used in group A, the mixed-cell injection demonstrated faster subcutaneous tumor growth, which indicated a tumor-promoting effect of the tumor-stromal interaction (Figure 6A). H&E staining revealed that both tumors contained a ductal structure with intervening stromal components, and no obvious difference was observed (Figure 6B).

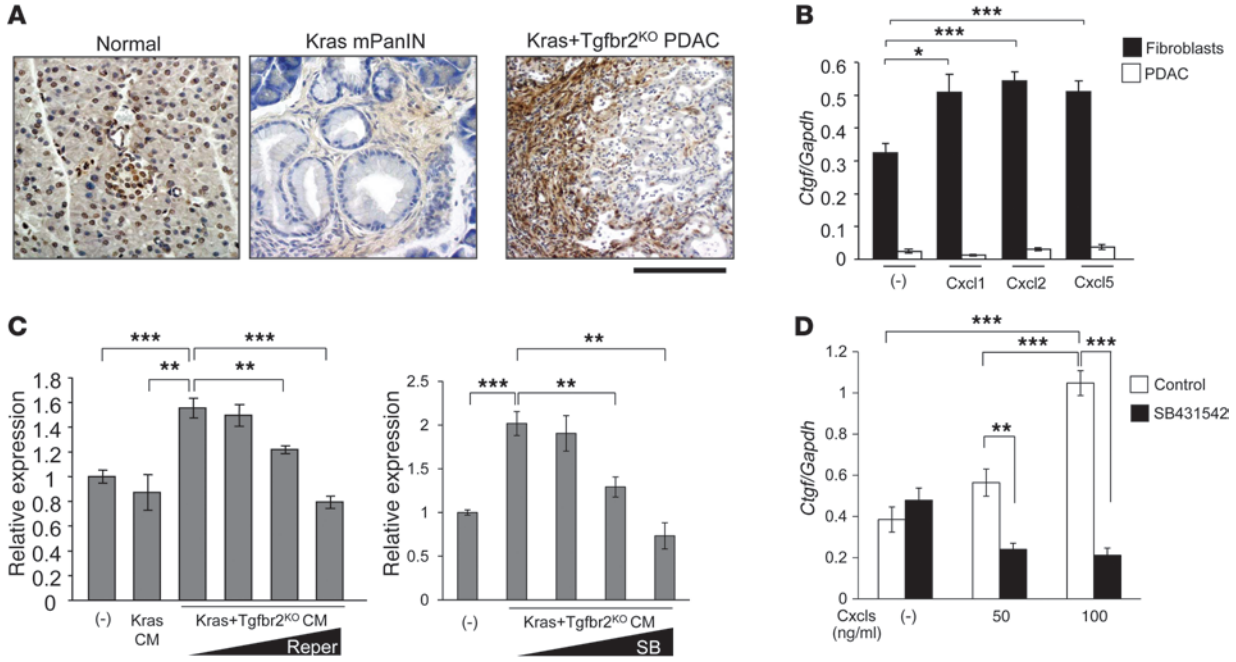

Figure 5

Cxc chemokines from Kras+Tgfbr2^{KO} PDAC cells induce Ctgf expression in pancreatic fibroblasts in the tumor microenvironment. (**A**) Representative figures from Ctgf immunohistochemistry. Ctgf was strongly expressed in the stromal area adjacent to the PDAC tumor epithelia and the tumor cells at the invasive front in Kras+Tgfbr2^{KO} mice. Scale bars: 125 μm. (**B**) QRT-PCR showed that *Ctgf* mRNA expression was significantly higher in the pancreatic fibroblasts than in Kras+Tgfbr2^{KO} PDAC cells, and the Cxc chemokines induced Ctgf expression in the fibroblasts. Cells were incubated with or without 100 ng/ml Cxcl1, -2, or -5 for 6 hours, then the RNA was extracted. The expression ratio of *Ctgf* to Gapdh is calculated. (**C**) QRT-PCR showed that CM from Kras+Tgfbr2^{KO} PDAC cells induced Ctgf expression in the pancreatic fibroblasts in a Cxcr2-dependent manner. Cells were incubated with the indicated CM and with various concentrations of repertaxin (Reper; 0.1–200 μM) or SB225002 (SB; 0.01–1 μM) for 6 hours, then the RNA was extracted. The data of cells without CM were set as 1. (**D**) QRT-PCR showed that the Cxcl-induced Ctgf upregulation in the pancreatic fibroblasts was TGF-β signal dependent. The pancreatic fibroblasts were incubated with or without Cxcl1, -2, and -5 (0–100 ng/ml each) and with or without 10 μM Tgfbr1 inhibitor SB431542 for 24 hours, then the RNA was extracted. The expression ratio of Ctgf to Gapdh was calculated. *$P < 0.05$; **$P < 0.01$; ***$P < 0.001$.

However, when we treated the mixed-cell tumors with the CXCR2 inhibitor repertaxin a significant growth-inhibitory effect was observed by week 4. The results suggested that the tumor-promoting effect of the observed tumor-stromal interaction was Cxcr2 dependent (Figure 6C). We further knocked down Cxcr2 in the PDAC cells or pancreatic fibroblasts, respectively, and made subcutaneous allografts by injecting with a combination of Cxcr2 wild-type PDAC cells and Cxcr2-knockdown fibroblasts (group C) or a combination of Cxcr2-knockdown PDAC cells and Cxcr2 wild-type fibroblasts (group D). Although the Cxcr2 knockdown did not affect in vitro cell proliferation or Cxcl expression in each cell type (Supplemental Figure 3), group C allografts showed significantly slower tumor growth compared with group D allografts (Figure 6D), which indicated that Cxcr2 knockdown in the stromal fibroblasts had a strong impact on tumor growth. More specifically, this tumor growth might be highly dependent on the axis of Cxcls from PDAC cells and Cxcr2 on the stromal fibroblasts, and thus the stromal Cxcr2 may be a more potent therapeutic target than epithelial Cxcr2 in the tumor-stromal interaction.

Treatment of the Ptf1a$^{cre/+}$;LSL-Kras$^{G12D/+}$;Tgfbr2$^{flox/flox}$ PDAC mice with Cxcr2 inhibitors demonstrate antitumor effects and prolong survival. Although informative, subcutaneous injection of tumor cells alone or in combination with other cell populations such as fibroblasts often fail to recapitulate many features and stepwise progression of human pancreatic cancer. Therefore, we examined the antitumor effect of Cxcl-Cxcr2 axis inhibition in a more clinically relevant setting by treating the *Ptf1a$^{cre/+}$;LSL-Kras$^{G12D/+}$;Tgfbr2$^{flox/flox}$* mice with repertaxin or SB225002. Since the tumors in this model grow rapidly and quickly lead to mortality, we started treatment at 3 weeks of age and continued treatment through 7 weeks of age, while the tumors remained viable. We also treated the mice with gemcitabine, a global standard chemotherapeutic reagent for PDAC, starting at 4 weeks of age with or without repertaxin as described above, through 7 weeks of age. This model required gemcitabine dose reduction because of the toxicity, from 50–100 mg/kg, which has been frequently used in xenograft studies, to 12.5 mg/kg. Compared with xenograft studies that usually use adult-stage mice, gemcitabine administration from much younger stages might result in more frequent and more severe toxic effects. Using the SB225002 inhibitor, we also examined the impact on overall survival in this model system.

When dissected, tumors often occupied most of the pancreas in control, repertaxin-treated, and SB225002-treated mice. However, we more frequently observed areas of morphologically normal pancreatic tissue in the treated groups, which suggested that the inhibitor delayed the tumor development (Figure 7A). When treated with gemcitabine, the tumor formation was obviously inhibited, demonstrating focal tumor areas and well-retained normal

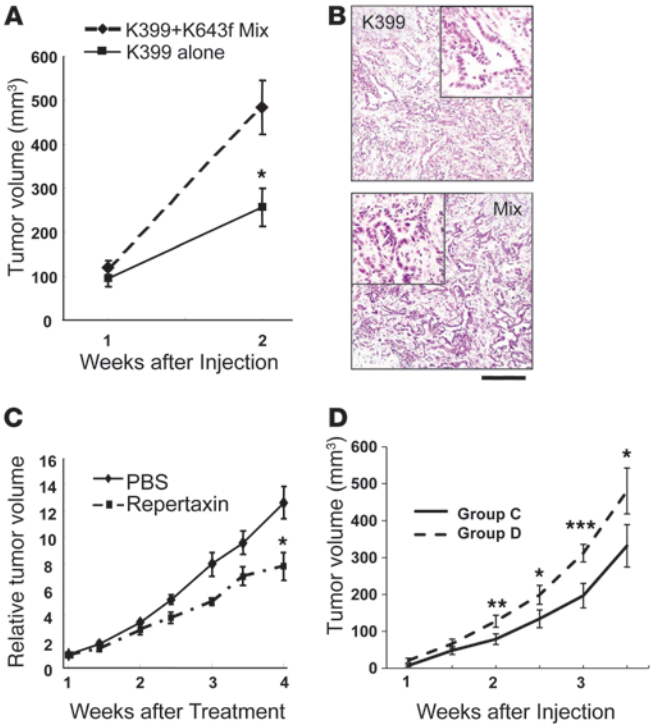

Figure 6
Tumor-stromal interaction accelerates PDAC progression in a Cxcr2-dependent manner in vivo. (**A**) Growth of subcutaneous tumor allograft. K399 PDAC cells (3×10^6) or a mixture of 1.5×10^6 PDAC cells and 1.5×10^6 K643f fibroblasts were subcutaneously injected into nude mice. The mixture showed faster tumor growth. n = 8/group. (**B**) H&E staining of subcutaneous tumors. Scale bar: 200 μm (insets, 100 μm). (**C**) Growth of subcutaneous mixed-cell tumor allograft with or without CXCR2 antagonist. A mixture of 1.5×10^6 K399 PDAC cells and 1.5×10^6 K643f fibroblasts was subcutaneously injected into nude mice, and 1 week later, 30 mg/kg repertaxin or PBS was injected subcutaneously 5 days/week. Inhibition of Cxcr2 slowed tumor growth. n = 7/group. Tumor volume of day 1 was assigned as 1, and relative volume is shown. (**D**) Growth of subcutaneous mixed-cell tumor allograft with or without Cxcr2 knockdown. A mixture of Cxcr2 wild-type PDAC cells (K399) and Cxcr2-knockdown fibroblasts (K643f) (1.0×10^6 each) (group C) or a mixture of Cxcr2-knockdown K399 and Cxcr2 wild-type K643f (1.0×10^6 each) (group D) was subcutaneously injected into nude mice. n = 12/group. Cxcr2 knockdown in fibroblasts slowed tumor growth. The tumor volume was calculated by the following equation: volume = $0.5 \times L \times W^2$. $^*P < 0.05$; $^{**}P < 0.01$; $^{***}P < 0.001$.

pancreas structure in the H&E staining (Figure 7A). Some necrotic areas were also observed in the pancreas of mice treated with gemcitabine. Importantly, morphologically normal pancreatic tissue was more frequently observed in the combination treatment with repertaxin and gemcitabine (Figure 7A). These histological observations reflected the gross appearance, which consisted of focal hard nodules and surrounding soft pancreatic tissue. Tumor volume was assessed by measuring the size of pancreas and revealed that repertaxin or SB225002 treatment alone significantly decreased the tumor volume, and adding gemcitabine resulted in further suppression (Figure 7A).

Previously, it was reported that the CXC chemokine ligands described above and CTGF enhanced angiogenesis in the tumor microenvironment (23, 28, 29). As shown in Figure 7B, microvessel density (MVD) of the CXCR2 inhibitor–treated group was significantly lower than that of the control group. Interestingly, the gemcitabine-treated group did not show obvious inhibition of angiogenesis. The combination therapy group of repertaxin and gemcitabine trended toward decreased MVD, although this observation was not statistically significant. Immunohistochemistry also revealed that Ctgf expression was decreased in the treatment group compared with the control (Figure 8A). Both CXCR2 inhibitors decreased Ctgf expression in the remaining stroma of PDAC tissue. In contrast, gemcitabine-treated tissues also showed a decrease in Ctgf expression that appeared to correlate with the observed decrease of stromal volume. Together, these results suggest that inhibition of the Cxcl-Cxcr2 axis decreased Ctgf expression and inhibited tumor angiogenesis, thereby suppressing tumor progression. The Cxcr2 inhibition also showed a significant apoptosis induction and decrease of PCNA labeling index (Supplemental Figure 4).

We also observed an increase in overall survival in mice treated with SB225002 that was statistically significant in a log-rank test (P = 0.0044), with a median survival of 62 days in the treated group versus 52 days in the control group (Figure 8B). The underlying mechanisms associated with suppression of PDAC progression via Cxcl-Cxcr2 inhibition and gemcitabine treatment appear to be unrelated, and the results suggest that combining these distinct antitumor agents may be a promising therapeutic strategy for PDAC. Therefore, we performed a survival study treating the mice with a combination of gemcitabine plus SB225002 or gemcitabine alone. The combination and gemcitabine-alone treatments showed significant survival extension compared with the control group (P = 0.0357 and P = 0.0200, respectively, in a log-rank test), with the same median survival of 57 days (Supplemental Figure 5). Unfortunately, the combination treatment did not show an advantage in the survival data compared with the single treatment (P = 0.728 versus SB225002 alone, P = 0.788 versus gemcitabine alone in a log-rank test) (Supplemental Figure 5). SB225002 and gemcitabine did not show statistical difference in the survival (P = 0.366). Some mice in the combination group lost body weight and died earlier than expected, which suggested similar toxicity as was observed in the gemcitabine treatment. Further dose reduction of gemcitabine might be required to obtain the optimum combination of SB225002 and gemcitabine.

Discussion

In the present study, we investigated tumor-stromal interactions in the *Ptf1a*$^{cre/+}$;*LSL-Kras*$^{G12D/+}$;*Tgfbr2*$^{flox/flox}$ mouse PDAC model. This model features differentiated ductal adenocarcinoma with abundant stromal components including the desmoplasia frequently observed in human PDAC tissue. Using this model, we found that the PDAC cells abundantly secreted several Cxc chemokines, most of which signal through Cxcr2. The Cxc chemokines produced by PDAC cells did not have an autocrine impact on tumor cell growth in vitro. However, mixing pancreatic fibro-

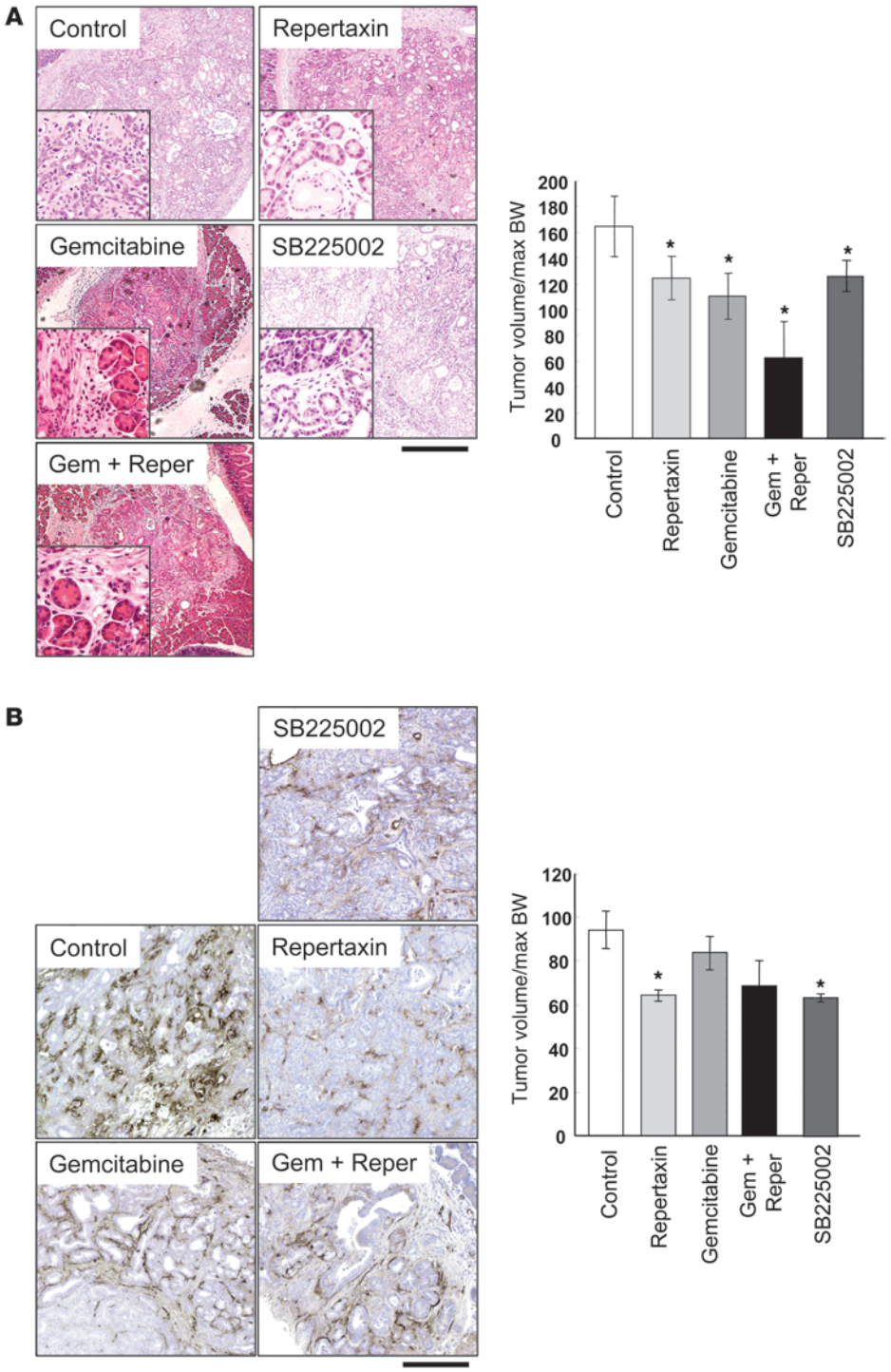

Figure 7
Blockade of the Cxcl-Cxcr2 axis shows an antitumor effect by reducing tumor angiogenesis on the Kras+Tgfbr2^{KO} PDAC mice. (**A**) H&E staining of the Kras+Tgfbr2^{KO} PDAC mouse treated with vehicle, repertaxin, gemcitabine, repertaxin plus gemcitabine, or SB225002. Scale bars: 400 μm (insets, 100 μm). Tumor size index in each treatment group was quantified (n = 6). (**B**) Immunohistochemistry of von Willebrand factor. Scale bars: 100 μm. MVD in each treatment group was quantified (n = 4). *P < 0.05 vs. control.

blasts with PDAC cells accelerated subcutaneous tumor growth in vivo, which was Cxcr2 dependent. Moreover, treating the *Ptf1a$^{cre/+}$;LSL-Kras$^{G12D/+}$;Tgfbr2$^{flox/flox}$* mice with CXCR2 inhibitor with or without gemcitabine demonstrated antitumor effects and extended survival. These effects correlated with decreased expression of Ctgf from the fibroblasts and reduced angiogenesis. Together, these results indicate that blockade of the Cxcl-Cxcr2 axis may be an effective adjuvant therapeutic strategy for PDAC.

Cxc chemokines are major factors mediating signals from the tumor cells in the tumor-stromal interaction from the early to advanced stages of PDAC progression. Abundance of stroma in Kras+Tgfbr2^{KO} PDAC, which recapitulated human PDAC, prompted us to investigate tumor-stromal interaction in the PDAC tissue. We tried to dissect the tumor-stromal interaction in the PDAC to elucidate how tumor cells stimulate the stroma and how stromal cells respond to the tumor cells.

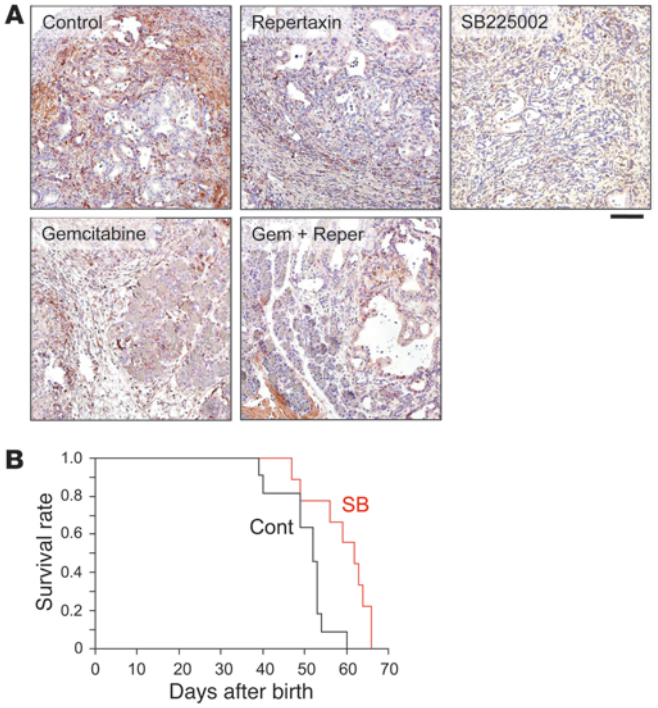

Figure 8

Treatment of Kras+Tgfbr2^{KO} PDAC mice with CXCR2 inhibitor decreases Ctgf expression and prolongs survival. (**A**) Immunohistochemistry of Ctgf. Scale bar: 100 μm. (**B**) Survival curve of Kras+Tgfbr2^{KO} PDAC mice treated with SB225002 vs. vehicle. Cont, control; SB, SB225002. Log-rank test demonstrated a statistically significant difference between the 2 groups (P = 0.0044).

First we screened secreted factors in the culture media of the Kras+Tgfbr2^{KO} PDAC cells, comparing them with those of the Kras-alone–activated mPanIN cells. We found that the Kras+Tgfbr2^{KO} PDAC cells characteristically produced and secreted several Cxc chemokines considered to be the major factors from the PDAC cells affecting the tumor microenvironment. Blockade of TGF-β signaling by knockout of Tgfbr2 dramatically enhanced PDAC progression and enhanced the Cxc chemokine production. This suggested that constitutive TGF-β signaling can regulate and prevent PDAC progression by inhibiting Cxc chemokine production. In the pancreatic cells with intact TGF-β signaling, Cxcl1 and -5 were downregulated by adding TGF-β1 ligand. This was also observed in breast cancer cells (30), which indicated that transcriptional regulation of those Cxc chemokines is a common mechanism that can have a significant impact on cancer progression.

Recently, it was reported that *KRAS*-alone–activated pancreatic ductal cells also showed enhanced CXCL1 and -5 expression compared with normal pancreatic ductal cells, and that human PDAC produces CXCL1, -5 and -8 with high levels of the chemokines in the pancreatic fluid (28, 29). CXCL1, -5, and -8 all signal through Cxcr2, although mice don't have the human CXCL8 ortholog.

In the *KRAS*-activated cells, the RAS-MAPK signal has been reported to induce CXCLs (28). Although Kras+Tgfbr2^{KO} PDAC has also shown strong phosphorylation of ERK (11), this study revealed that the NF-κB signal was the most highly involved in Cxcl1 and -5 upregulation among representative signal pathways including ERK, PI3K, p38MAPK, and JNK. It was reported that the CXCLs, known as pro-inflammatory cytokines, are regulated by NF-κB signaling (31) and that NF-κB signaling is constitutively activated in human PDAC cells (32). Moreover, TGF-β signaling was reported to inhibit NF-κB in other cell types (33, 34). There might be similar mechanisms at work in the PDAC cells in our study, which suggested that TGF-β signaling might have a crucial role against inflammation and cancer progression by inhibiting NF-κB signal.

Together, these results suggest that CXCL-CXCR2 signaling can contribute to human pancreatic carcinogenesis from the early PanIN stage to the advanced PDAC stage: initially, KRAS-MAPK activation induces the CXCLs in the early PanIN stage, and later, abrogation of TGF-β signaling further enhances CXCL production, which is dependent on active NF-κB signaling, resulting in advanced PDAC. Therefore, inhibition of RAS-MAPK and NF-κB signaling might be a possible therapeutic candidate.

Modulating Cxc chemokines, Ctgf and tumor angiogenesis in the tumor microenvironment is important in regulating PDAC progression as a therapeutic strategy. Since desmoplasia, fibrosis associated with invasive cancer, is a well-known hallmark of PDAC histology, we focused on the interaction between fibroblasts and PDAC cells in the present study. Strong expression of Ctgf protein, originally defined as a profibrotic factor, especially in the tumor-stromal border area of Kras+Tgfbr2^{KO} PDAC tissue also indicated active interaction between PDAC cells and fibroblasts. Thus we isolated pancreatic fibroblasts from the murine pancreas tissue and found that coexistence of pancreatic fibroblasts with PDAC cells accelerated tumor growth in vivo in a Cxcl-Cxcr2–dependent manner.

CXC chemokines were originally considered to be chemoattractants of neutrophils and recently have also been considered important in tumor progression (35). CXC chemokines are divided into 2 groups: the ELR motif–positive group, which induces angiogenesis, and the ELR motif–negative group, which is angiostatic. Most of the Cxc chemokines released from the PDAC cells here belonged to the ELR motif–positive group, which was reported to induce angiogenesis directly through proliferation and vascular tube formation of vascular endothelial cells (29, 36). In addition, we showed that the Cxc chemokines induced Ctgf expression in the pancreatic fibroblasts. CTGF is also considered to promote tumors through enhancement of tumor angiogenesis (23). Therefore, the Cxc chemokines from the Kras+Tgfbr2^{KO} PDAC cells might accelerate tumor progression through 2 synergistic actions: direct activation of vascular endothelial cells and induction of Ctgf expression in the fibroblasts. Treatment with CXCR2 inhibitors demonstrated reduced MVD and Ctgf expression.

It is well known that TGF-β signaling is a major inducer of CTGF expression (37). We observed in this study that Ctgf induction by the Cxc chemokines was also TGF-β signal dependent. Since we have shown that the level of TGF-β ligand was elevated in the Kras+Tgfbr2^{KO} PDAC tissues (11) and stromal cells have intact TGF-β signaling in the model, TGF-β may have clearly distinct roles between in the pancreatic epithelial cells and stromal cells — blockade of TGF-β signal in pancreatic epithelial cells dramatically accelerates Kras^{G12D}-induced PDAC formation, indicating a tumor-suppressive role of TGF-β, whereas intact and enhanced TGF-β signaling in stromal cells promotes CTGF expression, extracellular matrix production, and fibrosis, suggesting a central role of stromal expansion in the PDAC. It is well known that TGF-β has dual roles as a "Jekyll and Hyde," a tumor-inhibitory

effect in the early stage of cancer progression and a tumor-promoting effect in the advanced stage (38). Our observation might overlap with this: dramatic tumor progression upon the signal blockade in this context is consistent with the tumor-inhibitory effect in the early stage. On the other hand, enhanced signaling and stromal expansion are considered to be tumor-promoting effects in the later stage.

Recently Adrian et al. (39) documented that Tgfbr1 haploinsufficiency decreased incidence and tumor number of *Kras*-induced pancreatic precancer development, which is an opposite result from what we have reported in our model (11). The difference between the 2 models seems associated with the dual roles of TGF-β, especially the effects on the stroma. The model of Adrian et al. contains a heterozygous Tgfbr1 knockout both in the epithelium and stroma. In contrast, our model contains Tgfbr2 knockout only in the pancreatic epithelium. Therefore, intact TGF-β signaling in the stroma promotes stromal cell proliferation and deposition of extracellular matrices as well as Ctgf induction, together, in favor of tumor progression in our model. The histological images of pancreatic lesions of Adrian et al. appear to have much fewer stroma than the mPanIN-like lesions in our models (11), which seem consistent with this idea.

The Kras+Tgfbr2^{KO} PDAC tissues also demonstrated abundant macrophage infiltration. Tumor-associated macrophages have also been recognized as an important tumor-promoting component in the tumor microenvironment (40). The tumor-promoting effect is also considered to be tumor angiogenesis (41).

Thus, PDAC is well known as hypovascular in general, but angiogenesis might be invariably important for tumor progression, as higher levels of VEGF, a key molecule of angiogenesis, in the PDAC tissue are associated with poor prognosis (42). Cxcr2 inhibition did not directly inhibit cell proliferation of PDAC cells or fibroblasts, but it might have a significant impact on modulating an interplay of cell components in the tumor microenvironment, resulting in inhibition of angiogenesis and prolonged survival in this PDAC model. Very recently, Erez et al. reported that cancer-associated fibroblasts enhanced angiogenesis and tumor progression by secreting proinflammatory cytokines including angiogenic CXCLs in an NF-κB–dependent manner (43). The proinflammatory cytokines recruited macrophages into the tumor microenvironment, which mediated tumor-promoting inflammation and angiogenesis. Therefore, the antitumor effects and prolonged survival in this study might be products of inhibition of CXCLs, not only from PDAC cells but also from cancer-associated fibroblasts, that were highly involved in modulating an interplay of a wide variety of cell components in the tumor microenvironment. Our results also indicate that CXCR2 expression in the stroma might be more important than CXCR2 expression in the tumor epithelium. Thus, considering clinical settings, CXCR2 immunohistochemistry using surgical specimens or fine-needle biopsy samples of PDAC might be considered before treatment, and positive CXCR2 staining especially in the stromal area might be a determinant for personalized therapy with CXCR2 inhibition.

The antitumor mechanisms of gemcitabine and the CXCR2 inhibitor were obviously different. Pancreas of the mice treated with gemcitabine still retained normal structure with multiple tumor foci, while they did not show a decrease in MVD. In contrast, mice treated with CXCR2 inhibitor showed diffuse tumor formation in the pancreas with minimal normal area remaining and significantly decreased MVD. Therefore, the combination of gemcitabine, which inhibits DNA synthesis, mainly targeting tumor cells, and CXCR2 inhibitor, which mainly modulates tumor microenvironment and inhibits angiogenesis, might be a synergistic therapeutic strategy and may prevent excessive toxicities by allowing dose reduction of each drug.

We analyzed secreted factors from the PDAC cells and identified several Cxc chemokines. This is the first study that addressed key secreted factors from the PDAC cells into the microenvironment and showed therapeutic impact of blockade of Cxcl-Cxcr2 axis on PDAC. In conclusion, tumor-stromal interaction plays an important role in PDAC progression, in which the CXCL-CXCR2 axis and CTGF expression are highly involved. Therefore, combinations that target the interaction in the tumor microenvironment by blocking the axis as well as target tumor cells with chemoreagents like gemcitabine might be a potent synergistic strategy for PDAC therapy, and the optimum combination should be identified.

Methods

Mouse colonies. *Tgfbr2*$^{flox/flox}$ (44) and *Ptf1a*$^{cre/+}$ (45) mice were described previously. *LSL-Kras*$^{G12D/+}$ mice were a gift from Tyler Jacks (Massachusetts Institute of Technology, Cambridge, Massachusetts, USA) (46). The 3 lines were intercrossed to generate *Ptf1a*$^{cre/+}$;*LSL-Kras*$^{G12D/+}$;*Tgfbr2*$^{flox/flox}$ mice on a more than 95% C57BL/6 background. Genotyping of *Ptf1a*$^{cre/+}$, *LSL-Kras*$^{G12D/+}$, floxed *Tgfbr2* alleles was performed by using oligonucleotide primers as described previously (44–46).

Establishing primary pancreatic epithelial and fibroblast cell lines. Mouse pancreas epithelial cells and fibroblasts were separated and cultured in dishes coated with Vitrogen (Angiotech Biomaterials) and fibronectin (Sigma-Aldrich) in RPMI media (Sigma-Aldrich) supplemented with 20% FBS (HyClone) and antibiotics. Partial trypsinization was used for separating fibroblasts from epithelial cells. *Ptf1a*$^{cre/+}$;*LSL-Kras*$^{G12D/+}$;*Tgfbr2*$^{flox/flox}$ PDAC cell lines and *Ptf1a*$^{cre/+}$;*LSL-Kras*$^{G12D/+}$ mPanIN cell lines were established as described before (11), and the fibroblast population was obtained from *Ptf1a*$^{cre/+}$;*LSL-Kras*$^{G12D/+}$ mPanIN pancreas tissue. Fibroblasts were distinguished from the epithelial cells, characterized by PCR and cell staining. Genomic DNA of the cells was extracted and subjected to PCR for *LSL-Kras*^{G12D} and *Tgfbr2* recombined allele detection (7, 47). The fibroblasts were negative for *LSL-Kras*^{G12D} and *Tgfbr2* allele recombination in PCR. Immunofluorescence of ZO-1 and F-actin was performed as described previously (48) and demonstrated that fibroblasts had no cell junctional staining of ZO-1 (Chemicon International) but showed stress fiber formation stained with Texas Red–X phalloidin (Molecular Probes Inc.). Fibroblasts further showed abundant S100a4 and Ng2 protein expression in Western blot analysis.

Reagents. Recombinant mouse Cxcl1 (Kc), Cxcl2 (Mip-2), and Cxcl5 (Lix) were purchased from R&D Systems. Recombinant porcine TGF-β1 was obtained from R&D Systems. The allosteric CXCR2 inhibitor repertaxin was purchased from Sigma-Aldrich, and the CXCR2 inhibitor SB225002 was obtained from Calbiochem. The NF-κB inhibitor (IκB kinase-2 inhibitor) SC-514 and the Tgfbr1 inhibitor SB431542 were also obtained from Calbiochem.

Cytokine antibody array. Proteins secreted from the pancreatic tumor cells were screened by using the RayBio Mouse Cytokine Antibody Array C Series 1000 (RayBiotech Inc.) according to the manufacturer's instructions. In brief, 2 × 10^5 *Ptf1a*$^{cre/+}$;*LSL-Kras*$^{G12D/+}$;*Tgfbr2*$^{flox/flox}$ PDAC cells (4 lines) or *Ptf1a*$^{cre/+}$;*LSL-Kras*$^{G12D/+}$ mPanIN cells (3 lines) were seeded into a 10-cm dish. On the next day, culture medium was changed for a new medium with 5% FBS, and cells were cultured for an additional 24 hours. Then the CM was collected, filtered, and subjected to the antibody array incubation. The amount of CM used was normalized by the cell number. The membranes were washed and incubated with primary biotin-conjugated antibody and then incubated with horseradish peroxidase–conjugated streptavidin, and

the protein spots were detected using the ECL Western blotting detection reagents (GE Healthcare) according to the manufacturer's instructions. The spot density was quantified and compared between the PDAC cells and mPanIN cells. A complete list of the molecules examined by cytokine antibody array is shown in Supplemental Table 1.

Histology and immunohistochemistry. Mouse tissue was harvested and processed as described before (11). Trichrome Blue staining and immunohistochemistry for α–smooth muscle actin and F4-80 were performed in the Vanderbilt Histology Core Facility. Other staining was performed using Cxcl1 rat monoclonal (1:200 dilution; R&D Systems), Cxcr2 goat polyclonal (1:100; Santa Cruz Biotechnology Inc.), S100a4 rabbit polyclonal (1:1500; DakoCytomation), Ng2 rabbit polyclonal (1:500; Chemicon International), and von Willebrand factor rabbit polyclonal (1:500; DakoCytomation) antibodies, respectively. They were stained by biotinylated secondary antibodies (Vector Laboratories) and followed using Elite Vectastain ABC kit (Vector Laboratories) and peroxidase substrate DAB kit (Vector Laboratories). Antigen retrieval was performed in all experiments. For Ctgf staining, Ctgf mouse monoclonal antibody was provided by FibroGen Inc. (23) and staining was performed according to the manufacturer's instruction.

QRT-PCR. RNA was extracted from the primary pancreas cell lines using TRIzol (Invitrogen) and treated with RQ1 DNase (Promega), and then cDNA was made from 0.5 μg of total RNA using Superscript II reverse transcriptase (Invitrogen) according to the manufacturer's instructions. QRT-PCR was performed using iQ SYBR Green Supermix (Bio-Rad) and iQ Cycler (Bio-Rad) according to the manufacturer's instructions. Relative expression was calculated as a ratio of the particular gene expression to *Gapdh* expression.

For TGF-β1 treatment, *Ptf1a*$^{cre/+}$;*LSL-Kras*$^{G12D/+}$ mPanIN cells were incubated with or without 5 ng/ml TGF-β1 for 6 hours and RNA was extracted as described above to examine Cxc chemokine expression. Cxcl1 and -5 expression was also examined using the *Ptf1a*$^{cre/+}$;*LSL-Kras*$^{G12D/+}$;*Tgfbr2*$^{flox/flox}$ PDAC cells incubated with the NF-κB inhibitor (IκB kinase-2 inhibitor) SC-514 (50–100 μM) for 12 hours. We also examined other signal inhibitors as described in the Supplemental Methods.

For Cxc chemokine treatment, PDAC cells and fibroblasts were incubated for 6 hours with or without 100 ng/ml Cxcl1, Cxcl2, or Cxcl5, and then RNA was extracted to examine Ctgf expression.

Ctgf expression was also examined in the fibroblasts with or without the pancreatic epithelial cell CM. The fibroblasts were incubated with *Ptf1a*$^{cre/+}$;*LSL-Kras*$^{G12D/+}$;*Tgfbr2*$^{flox/flox}$ PDAC cell CM, *Ptf1a*$^{cre/+}$;*LSL-Kras*$^{G12D/+}$ mPanIN cell CM, or CM alone (control) for 6 hours, then subjected to RNA extraction. To determine Cxcr2 dependency, the fibroblasts were incubated with *Ptf1a*$^{cre/+}$;*LSL-Kras*$^{G12D/+}$;*Tgfbr2*$^{flox/flox}$ PDAC cell CM and various concentrations of CXCR2 inhibitor repertaxin (0.1 to 200 μM) or SB225002 (10 nM to 1 μM) for 6 hours, and RNA was extracted. Ctgf expression was also examined in the fibroblasts incubated with or without Cxcl1, -2, and -5 (0–100 ng/ml each) and with or without 10 μM Tgfbr1 inhibitor SB431542 for 24 hours. Sequences of the primers used are shown in Supplemental Table 2.

Western blotting. Total lysates of primary pancreatic cell lines were extracted and Western blot was performed as described before (11). Primary antibodies used were: S100a4 at 1:1,000 dilution (DakoCytomation), Ng2 at 1:1,000 (Chemicon International), and β-tubulin at 1:500 (obtained as described previously) (49).

Cell proliferation assay. In vitro cell proliferation assay was performed using Cell Counting Kit-8 (Dojindo) according to the manufacturer's instructions. Briefly, cells were plated in triplicate in 48-well dishes (Iwaki). The next day, CXCR2 inhibitor SB225002 was added at various concentrations (0–1 μM) and the cells were incubated for 0–48 hours. For the last 3 hours of incubation, cells were pulsed with 10 μl CCK8 reagent (Dojindo) into 100 μl of culture media, and then absorbance of 450 nm was measured.

Subcutaneous tumor grafting study. Six-week-old female Balb/c athymic mice were subcutaneously injected with the following murine pancreatic cells: Group A, 3 × 10^6 cells from the *Ptf1a*$^{cre/+}$;*LSL-Kras*$^{G12D/+}$;*Tgfbr2*$^{flox/flox}$ PDAC cell line K399 (n = 8); Group B, a mixture of 1.5 × 10^6 K399 PDAC cells and 1.5 × 10^6 K643f pancreatic fibroblasts separated from the *Ptf1a*$^{cre/+}$;*LSL-Kras*$^{G12D/+}$ mouse pancreas (n = 8). Tumor volume was determined by external measurement and calculated according to the equation $V = 0.5 \times [LW^2]$, where V indicates volume, L indicates length, and W indicates width.

For the Cxcr2 inhibition study, subcutaneous tumors were made by injecting the mixture of K399 PDAC and K643f fibroblasts as described above; 1 week later, subcutaneous treatment was begun 5 days/week with PBS as vehicle or 30 mg/kg repertaxin (Sigma-Aldrich) (n = 7). The tumor volume was calculated and compared as described above.

To determine the importance of Cxcr2 activity in the PDAC cells or the pancreatic fibroblasts on the tumor growth, knockdown of Cxcr2 in either the PDAC cells or the pancreatic fibroblasts was performed (described in detail in the Supplemental Methods). Subcutaneous allografts were made by injecting a combination of Cxcr2 wild-type PDAC cells K399 and Cxcr2-knockdown pancreatic fibroblasts K643f (group C) or a combination of Cxcr2-knockdown K399 and Cxcr2 wild-type K643f (group D) (n = 12 each), and tumor volume was compared as described above.

Treating mice bearing autochthonous PDAC. *Ptf1a*$^{cre/+}$;*LSL-Kras*$^{G12D/+}$;*Tgfbr2*$^{flox/flox}$ mice were treated with repertaxin (Sigma-Aldrich) or SB225002 (Calbiochem) as follows: PBS as vehicle or 15 mg/kg repertaxin was intraperitoneally injected 5 days/week, starting at 3 weeks of age. After 4 weeks of treatment, mice were euthanized and dissected. Cotreatment of repertaxin and gemcitabine (Eli Lilly and Co.) was also performed. In addition to repertaxin treatment, 12.5 mg/kg gemcitabine was injected intraperitoneally twice a week, starting at 4 weeks of age. After 3 weeks of treatment with gemcitabine (that is, after 4 weeks of treatment with repertaxin), the mice were euthanized and dissected. At this stage, most of the pancreas was already occupied by tumor. Width, height, and depth of the pancreas were measured, and the index of the pancreas size was calculated according to the following equation: index = $W \times H \times D$. Tumor volume was evaluated as a ratio of the size index to whole body mass (maximum body weight during the course of the experiment). The tumor tissue was processed as described above for further histological and immunohistochemical examinations.

Similarly, mice were treated with SB225002, which was suspended in 0.25% Tween-20 (WAKO) in PBS. The vehicle or 0.5 mg/kg SB225002 was injected intraperitoneally 5 days/week, starting at 3 weeks of age. Cotreatment with gemcitabine and the successive processes were performed in the same manner as for repertaxin, described above.

Median survival time was also analyzed. Treatment with gemcitabine, SB225002, a combination of the two, or vehicle control was performed as described above, and mice were kept under cautious observation. The survival data was analyzed using the log-rank test with JMP7 software (SAS).

MVD analysis. von Willebrand factor was immunostained as described above to quantitate the tumor MVD (50). Three fields with dense positive signals (×100 magnification) were chosen from each tumor, and each isolated positive signal was counted as a microvessel. The highest count of each tumor was adopted as the MVD.

Statistics. Except where indicated, quantitative data are presented as mean ± SEM, and the 2-sided Student's t test was used for statistical analysis, with $P < 0.05$ taken as significant.

Study approval. All animal experimental protocols were approved by the IACUC of Vanderbilt University or the ethics committee for animal experimentation at the Graduate School of Medicine, University of Tokyo, and conducted in accordance with the Association for the Assessment and Accreditation of Laboratory Animal Care guidelines of Vanderbilt University or the Guidelines for the Care and Use of Laboratory Animals of the University of Tokyo.

Acknowledgments

We thank the Vanderbilt immunohistochemistry core and tissue acquisition core laboratories; Mitsunobu R. Kano; Yasuyuki Morishita for histological, pathological advice, and assistance; Kohei Miyazono for handling reagents; and Mitsuko Tsubouchi for technical assistance. This work was supported by NIH grants CA085492, CA102162, and U54126505 to H.L. Moses; grants from the Japanese Ministry of Education, Culture, Sports, Science, and Technology (MEXT) to M. Omata and H. Ijichi; and grants from the Japanese Pancreatic Research Foundation, Sankyo Foundation of Life Science, Foundation for Promotion of Cancer Research in Japan, and Japanese Society of Gastroenterology to H. Ijichi.

Received for publication April 18, 2011, and accepted in revised form July 27, 2011.

Address correspondence to: Hideaki Ijichi, Department of Gastroenterology, Graduate School of Medicine, University of Tokyo, 7-3-1 Hongo, Bunkyo-ku, Tokyo 113-8655, Japan. Phone: 81.3.3815.5441; Fax: 81.3.3814.0021; E-mail: hideijichi-gi@umin.ac.jp.

1. Jemal A, Siegel R, Ward E, Murray T, Xu J, Thun MJ. Cancer statistics, 2007. *CA Cancer J Clin*. 2007; 57(1):43–66.
2. Matsuno S, et al. Pancreatic Cancer Registry in Japan: 20 years of experience. *Pancreas*. 2004; 28(3):219–230.
3. Warshaw AL, Fernandez-del Castillo C. Pancreatic carcinoma. *N Engl J Med*. 1992;326(7):455–465.
4. Bardeesy N, DePinho RA. Pancreatic cancer biology and genetics. *Nat Rev Cancer*. 2002;2(12):897–909.
5. Hruban RH, et al. Pancreatic intraepithelial neoplasia: a new nomenclature and classification system for pancreatic duct lesions. *Am J Surg Pathol*. 2001;25(5):579–586.
6. Rozenblum E, et al. Tumor-suppressive pathways in pancreatic carcinoma. *Cancer Res*. 1997; 57(9):1731–1734.
7. Hingorani SR, et al. Preinvasive and invasive ductal pancreatic cancer and its early detection in the mouse. *Cancer Cell*. 2003;4(6):437–450.
8. Aguirre AJ, et al. Activated Kras and Ink4a/Arf deficiency cooperate to produce metastatic pancreatic ductal adenocarcinoma. *Genes Dev*. 2003; 17(24):3112–3126.
9. Hingorani SR, et al. Trp53R172H and KrasG12D cooperate to promote chromosomal instability and widely metastatic pancreatic ductal adenocarcinoma in mice. *Cancer Cell*. 2005;7(5):469–483.
10. Bardeesy N, et al. Both p16(Ink4a) and the p19(Arf)-p53 pathway constrain progression of pancreatic adenocarcinoma in the mouse. *Proc Natl Acad Sci U S A*. 2006;103(15):5947–5952.
11. Ijichi H, et al. Aggressive pancreatic ductal adenocarcinoma in mice caused by pancreas-specific blockade of transforming growth factor-beta signaling in cooperation with active Kras expression. *Genes Dev*. 2006;20(22):3147–3160.
12. Jones S, et al. Core signaling pathways in human pancreatic cancers revealed by global genomic analyses. *Science*. 2008;321(5897):1801–1806.
13. Wagner M, Kleeff J, Friess H, Buchler MW, Korc M. Enhanced expression of the type II transforming growth factor-beta receptor is associated with decreased survival in human pancreatic cancer. *Pancreas*. 1999;19(4):370–376.
14. Venkatasubbarao K, et al. Differential expression of transforming growth factor beta receptors in human pancreatic adenocarcinoma. *Anticancer Res*. 2000;20(1A):43–51.
15. Bardeesy N, et al. Smad4 is dispensable for normal pancreas development yet critical in progression and tumor biology of pancreas cancer. *Genes Dev*. 2006;20(22):3130–3146.
16. Izeradjene K, et al. Kras(G12D) and Smad4/Dpc4 haploinsufficiency cooperate to induce mucinous cystic neoplasms and invasive adenocarcinoma of the pancreas. *Cancer Cell*. 2007;11(3):229–243.
17. Kojima K, et al. Inactivation of Smad4 accelerates Kras(G12D)-mediated pancreatic neoplasia. *Cancer Res*. 2007;67(17):8121–8130.
18. Olive KP, et al. Inhibition of Hedgehog signaling enhances delivery of chemotherapy in a mouse model of pancreatic cancer. *Science*. 2009;324(5933):1457–1461.
19. Mueller MM, Fusenig NE. Friends or foes - bipolar effects of the tumour stroma in cancer. *Nat Rev Cancer*. 2004;4(11):839–849.
20. Kalluri R, Zeisberg M. Fibroblasts in cancer. *Nat Rev Cancer*. 2006;6(5):392–401.
21. Mahadevan D, Von Hoff DD. Tumor-stroma interactions in pancreatic ductal adenocarcinoma. *Mol Cancer Ther*. 2007;6(4):1186–1197.
22. Jimenez RE, Hartwig W, Antoniu BA, Compton CC, Warshaw AL, Fernández-Del Castillo C. Effect of matrix metalloproteinase inhibition on pancreatic cancer invasion and metastasis: an additive strategy for cancer control. *Ann Surg*. 2000;231(5):644–654.
23. Aikawa T, Gunn J, Spong SM, Klaus SJ, Korc M. Connective tissue growth factor-specific antibody attenuates tumor growth, metastasis, and angiogenesis in an orthotopic mouse model of pancreatic cancer. *Mol Cancer Ther*. 2006;5(5):1108–1116.
24. Dornhofer N, et al. Connective tissue growth factor-specific monoclonal antibody therapy inhibits pancreatic tumor growth and metastasis. *Cancer Res*. 2006;66(11):5816–5827.
25. Kang Y, et al. A multigenic program mediating breast cancer metastasis to bone. *Cancer Cell*. 2003;3(6):537–549.
26. Bennewith KL, et al. The role of tumor cell-derived connective tissue growth factor (CTGF/CCN2) in pancreatic tumor growth. *Cancer Res*. 2009;69(3):775–784.
27. Bertini R, et al. Noncompetitive allosteric inhibitors of the inflammatory chemokine receptors CXCR1 and CXCR2: prevention of reperfusion injury. *Proc Natl Acad Sci U S A*. 2004;101(32):11791–11796.
28. Matsuo Y, et al. K-Ras promotes angiogenesis mediated by immortalized human pancreatic epithelial cells through mitogen-activated protein kinase signaling pathways. *Mol Cancer Res*. 2009; 7(6):799–808.
29. Matsuo Y, et al. CXC-chemokine/CXCR2 biological axis promotes angiogenesis in vitro and in vivo in pancreatic cancer. *Int J Cancer*. 2009;125(5):1027–1037.
30. Bierie B, et al. Abrogation of TGF-beta signaling enhances chemokine production and correlates with prognosis in human breast cancer. *J Clin Invest*. 2009;119(6):1571–1582.
31. Richmond A. Nf-kappa B, chemokine gene transcription and tumour growth. *Nat Rev Immunol*. 2002;2(9):664–674.
32. Fujioka S, et al. Function of nuclear factor kappaB in pancreatic cancer metastasis. *Clin Cancer Res*. 2003;9(1):346–354.
33. Shier MK, et al. Correlation of TGF beta 1 overexpression with down-regulation of proliferation-inducing molecules in HPV-11 transformed human tissue xenografts. *Anticancer Res*. 1999;19(6B):4969–4976.
34. Ruiz PA, Shkoda A, Kim SC, Sartor RB, Haller D. IL-10 gene-deficient mice lack TGF-beta/Smad-mediated TLR2 degradation and fail to inhibit proinflammatory gene expression in intestinal epithelial cells under conditions of chronic inflammation. *Ann N Y Acad Sci*. 2006;1072:389–394.
35. Strieter RM, Burdick MD, Mestas J, Gomperts B, Keane MP, Belperio JA. Cancer CXC chemokine networks and tumour angiogenesis. *Eur J Cancer*. 2006;42(6):768–778.
36. Strieter RM, et al. The functional role of the ELR motif in CXC chemokine-mediated angiogenesis. *J Biol Chem*. 1995;270(45):27348–27357.
37. Grotendorst GR. Connective tissue growth factor: a mediator of TGF-beta action on fibroblasts. *Cytokine Growth Factor Rev*. 1997;8(3):171–179.
38. Bierie B, Moses HL. Tumour microenvironment: TGFbeta: the molecular Jekyll and Hyde of cancer. *Nat Rev Cancer*. 2006;6(7):506–520.
39. Adrian K, et al. Tgfbr1 haploinsufficiency inhibits the development of murine mutant Kras-induced pancreatic precancer. *Cancer Res*. 2009;69(24):9169–9174.
40. Pollard JW. Tumour-educated macrophages promote tumour progression and metastasis. *Nat Rev Cancer*. 2004;4(1):71–78.
41. Condeelis J, Pollard JW. Macrophages: obligate partners for tumor cell migration, invasion, and metastasis. *Cell*. 2006;124(2):263–266.
42. Garcea G, Neal CP, Pattenden CJ, Steward WP, Berry DP. Molecular prognostic markers in pancreatic cancer: a systematic review. *Eur J Cancer*. 2005;41(15):2213–2236.
43. Erez N, Truitt M, Olson P, Hanahan D. Cancer-associated fibroblasts are activated in incipient neoplasia to orchestrate tumor-promoting inflammation in an NF-kappaB-dependent manner. *Cancer Cell*. 2010;17(2):135–147.
44. Chytil A, Magnuson MA, Wright CV, Moses HL. Conditional inactivation of the TGF-beta type II receptor using Cre:Lox. *Genesis*. 2002;32(2):73–75.
45. Kawaguchi Y, Cooper B, Gannon M, Ray M, MacDonald RJ, Wright CV. The role of the transcriptional regulator Ptf1a in converting intestinal to pancreatic progenitors. *Nat Genet*. 2002;32(1):128–134.
46. Jackson EL, et al. Analysis of lung tumor initiation and progression using conditional expression of oncogenic K-ras. *Genes Dev*. 2001;15(24):3243–3248.
47. Cheng N, et al. Loss of TGF-beta type II receptor in fibroblasts promotes mammary carcinoma growth and invasion through upregulation of TGF-alpha-, MSP- and HGF-mediated signaling networks. *Oncogene*. 2005;24(32):5053–5068.
48. Brown KA, et al. Induction by transforming growth factor-beta1 of epithelial to mesenchymal transition is a rare event in vitro. *Breast Cancer Res*. 2004;6(3):R215–R231.
49. Forrester E, et al. Effect of conditional knockout of the type II TGF-beta receptor gene in mammary gland development and polyomavirus middle T antigen induced tumor formation and metastasis. *Cancer Res*. 2005;65(6):2296–2302.
50. Weidner N. Intratumor microvessel density as a prognostic factor in cancer. *Am J Pathol*. 1995; 147(1):9–19.